A Nonlocal SAR image denoising algorithm based on LLMMSE wavelet shrinkage

Article *in* IEEE Transactions on Geoscience and Remote Sensing · February 2012

DOI: 10.1109/TGRS.2011.2161586 · Source: DBLP

4 authors:

S. Parrilli
CIRA Centro Italiano Ricerche Aerospaziali
18 PUBLICATIONS **252** CITATIONS
SEE PROFILE

Mariana Poderico
CIRA Centro Italiano Ricerche Aerospaziali
12 PUBLICATIONS **171** CITATIONS
SEE PROFILE

Cesario Vincenzo Angelino
CIRA Centro Italiano Ricerche Aerospaziali
24 PUBLICATIONS **167** CITATIONS
SEE PROFILE

Luisa Verdoliva
University of Naples Federico II
95 PUBLICATIONS **753** CITATIONS
SEE PROFILE

A Nonlocal SAR Image Denoising Algorithm Based on LLMMSE Wavelet Shrinkage

Sara Parrilli, Mariana Poderico, Cesario Vincenzo Angelino, and Luisa Verdoliva

***Abstract*—We propose a novel despeckling algorithm for synthetic aperture radar (SAR) images based on the concepts of nonlocal filtering and wavelet-domain shrinkage. It follows the structure of the block-matching 3-D algorithm, recently proposed for additive white Gaussian noise denoising, but modifies its major processing steps in order to take into account the peculiarities of SAR images. A probabilistic similarity measure is used for the block-matching step, while the wavelet shrinkage is developed using an additive signal-dependent noise model and looking for the optimum local linear minimum-mean-square-error estimator in the wavelet domain. The proposed technique compares favorably w.r.t. several state-of-the-art reference techniques, with better results both in terms of signal-to-noise ratio (on simulated speckled images) and of perceived image quality.**

***Index Terms*—Empirical Wiener filtering, linear minimum-mean-square-error (LMMSE) filtering, nonlocal filtering, speckle, synthetic aperture radar (SAR), undecimated discrete wavelet transform (UDWT).**

I. Introduction

SYNTHETIC aperture radar (SAR) images are inherently affected by speckle noise, which is due to the coherent nature of the scattering phenomena. Even though speckle carries itself information about the illuminated area, it degrades the appearance of images and affects the performance of scene analysis tasks carried out by computer programs (e.g., segmentation and classification) or even by human interpreters [1]. To counter this problem, users resort often to the multilook technique, which amounts to incoherently averaging a certain number (defined by the *number of looks*) of independent images, thus reducing noise intensity, but often at the cost of a clear loss in image resolution. Therefore, it is certainly preferable to develop suitable filtering techniques, which reduce noise significantly but, at the same time, preserve all the relevant scene features, such as radiometric and textural information.

Some of the early speckle reduction techniques (see, e.g., [2] and [3]) use the so-called homomorphic approach, taking the log of the data, so as to obtain a more tractable additive model, and then applying some well-known method drawn from the additive white Gaussian noise (AWGN) denoising literature. Although this approach has the undeniable merit of simplicity, it is necessarily suboptimal as it neglects some basic properties of speckle. In fact, the log-transformed speckle is non-Gaussian, markedly so in the important single-look case [4], and has nonzero mean, in general, a bias to be corrected before any other processing. More important, the logarithm changes radically the data dynamics, leading to unavoidable radiometric distortions during the denoising process.

In the same period, more ambitious techniques [5]–[10] tackle despeckling in the original domain (non-log-transformed), as a statistical estimation problem, based on the multiplicative speckle model. All such techniques operate in the spatial domain with linear filters developed under a minimum-mean-square-error (MMSE) approach. These early papers make already clear that some form of local adaptivity is necessary to account for the nonstationarity of the image: The intense smoothing required to reduce speckle in homogeneous areas cannot be applied in edge and textured regions lest important structural information gets lost. In [11]–[13], the simple MMSE estimation is replaced by the more sophisticated and promising maximum *a posteriori* (MAP) approach which, however, brings with it the problem of providing an accurate statistical description of the SAR image.

The diffusion of wavelets in the signal processing community, in the early 1990s, opens the way to a new generation of despeckling techniques operating in the transform domain. Indeed, wavelet shrinkage image denoising, based on AWGN hypothesis, has been one of the first and most successful applications of this transform. Wavelet shrinkage can be readily applied to SAR despeckling after a homomorphic transformation which leads to an additive noise model. This approach is followed in [14], and again in [15], where both hard and soft thresholding are tested. Despite the empirical selection of the threshold, experiments, on both synthetic and real SAR images, show already a clear performance gain w.r.t. spatial-domain adaptive filters. Further improvements are obtained by optimizing the shrinkage parameter through a statistical Bayesian approach [16]–[18]. Finally, like in the spatial domain, more sophisticated techniques [19]–[22] resort to the additive signal-dependent speckle model in order to overcome the drawbacks of the homomorphic approach.

All the wavelet-based techniques, like the classical spatial-domain techniques, embody some forms of spatial adaptivity in the filtering process in order to better preserve image boundaries and textures. This is also clear in some recent papers [23], [24] which resort to second-generation wavelet to better

Manuscript received November 16, 2010; revised April 28, 2011; accepted June 12, 2011. Date of publication August 18, 2011; date of current version January 20, 2012.

S. Parrilli, M. Poderico, and L. Verdoliva are with the Department of Biomedical, Electronic, and Telecommunication Engineering, University of Naples Federico II, 80121 Naples, Italy (e-mail: sara.parrilli@unina.it; mariana.poderico@unina.it; verdoliv@unina.it).

C. V. Angelino is with the Department of Biomedical, Electronic, and Telecommunication Engineering, University of Naples Federico II, 80121 Naples, Italy, and also with Laboratory I3S, University of Nice—Sophia Antipolis/CNRS, 06903 Sophia Antipolis, France (e-mail: cesariovincenzo.angelino@unina.it).

Digital Object Identifier 10.1109/TGRS.2011.2161586

represent edges and details of arbitrary spatial orientation. Therefore, detail preservation keeps being the main issue in SAR despeckling.

Given these premises, the nonlocal approach, recently proposed in [25] for AWGN denoising, looks like a potential breakthrough. The basic idea is to take advantage of the self-similarity commonly present in natural as well as SAR images: Certain image patches tend to repeat over and over, with minor modifications, throughout the scene, a circumstance to be exploited in view of the boundary preservation goal. In the nonlocal means (NLM) algorithm [25], filtering is carried out, as usual, through the weighted mean of all the pixels in a certain neighborhood. The weight associated with each given pixel, however, depends not on its geometrical distance from the target pixel but on its similarity with it. This similarity is then measured by the Euclidean distance between the patches surrounding the selected and the target pixels. This principle has inspired several extensions, among which the evolution toward a multipoint rather than pointwise filtering, as proposed in the block-matching 3-D (BM3-D) algorithm [26] where the nonlocal approach is combined with wavelet shrinkage and Wiener filtering in a two-step process. At present, BM3-D can be arguably [27] considered the state of the art for AWGN denoising.

The NLM algorithm has been readily extended to SAR despeckling [28]–[30] with suitable modifications aimed at taking into account the problem peculiarities. The probabilistic patch-based (PPB) algorithm [30] is particularly interesting, both for its theoretical contribution, with the development of a similarity measure well suited to SAR images, and for the excellent performance on test images.

Based on the conceptual path described earlier, and the related experimental evidence, in this work, we go one step further and propose a SAR-oriented version of BM3-D, with the obvious goal of replicating the competitive advantage it enjoys in the AWGN context. By taking into account the peculiar features of SAR images in the original domain, we derive a new[1] despeckling algorithm, called SAR-BM3-D from now on, which exhibits an objective performance comparable or superior to all competing techniques on simulated speckled images and guarantees a very good subjective quality on actual SAR images. Major innovative contributions w.r.t. the original BM3-D consist in the following: 1) using an *ad hoc* measure, inspired to [30], to form groups of similar image blocks; 2) resorting to local linear MMSE (LLMMSE) estimation criterion in the shrinkage phase; and 3) using undecimated wavelet to improve estimation reliability.

This paper is organized as follows. In Section II, we delineate the rationale and structure of BM3-D and motivate all modifications necessary to adapt the algorithm to handle speckled images. Then, in Section III, starting from the multiplicative noise model, the proposed improvements are rigorously and thoroughly described. Finally, in Section IV, we show the experimental results both on simulated and real SAR images.

[1]Preliminary results of the proposed technique are reported in [31].

II. BM3-D Algorithm and Its SAR-Oriented Version

The despeckling algorithm we propose here can be seen as a SAR-oriented version of BM3-D, since we use the same algorithmic structure as the original BM3-D but modify most of the individual processing steps in order to take into account the peculiarities of SAR data. Therefore, ideas and tools come from both the AWGN denoising and the SAR despeckling fields. In the following of this section, based on a high-level description of BM3-D ideas and algorithmic structure, we justify and briefly outline the major modifications that lead to its SAR-oriented version, leaving for the next section all detailed developments.

A. BM3-D

Under some restrictive conditions, the AWGN denoising problem has simple solutions. For example, if the source is wide-sense stationary, with perfectly known statistics, the optimum linear MMSE estimator is the well-known Wiener filter. Unfortunately, real-world images are *never* stationary (the information actually lies in nonstationarities), and their statistics are not easily estimated from noisy sources, which is why more sophisticated techniques are needed.

The wavelet transform (WT) represented a major step forward in this direction. In fact, WT provides a sparse representation of images [32] where large detail coefficients are associated with region boundaries, while small ones contain mostly noise. Therefore, some simple form of coefficient thresholding allows for a strong noise rejection with a good preservation of image details.

Shortly after Donoho first introduced wavelet shrinkage [33], Ghael *et al.* proposed [34] a two-step filtering procedure in the wavelet domain, which will be later reprised in BM3-D. The first step is a hard thresholding which provides a basic estimate of the clean image; such an estimate, however, is used only to compute the statistics for an empirical Wiener filtering operating in the transform domain [34] which performs the actual denoising of the original image. Back to Wiener, then, but in the transform domain and with a preliminary hard thresholding that provides the basis for better estimating the relevant statistics.

A further change of perspective came with the nonlocal filtering approach, recently introduced by Buades *et al.* [25], inspired by image in-painting literature [35] and by early work on neighborhood filters [36]. The nonlocal approach relies on the observation that most images exhibit clear self-similarities, as most patches repeat almost identically over and over in the image. Once these similar patches are identified, one can carry out the filtering along such patches, wherever they are, rather than in a local neighborhood of the pixel, mimicking a true statistical, as opposed to spatial, filtering.

The BM3-D algorithm [26] operates a very effective synthesis of all these ideas. Just like in [34], it works in two steps: The first one uses hard thresholding to build a relatively clean image for estimating statistics, while the second one performs the actual denoising through empirical Wiener filtering in the transform domain. Both steps, however, work not on local

neighborhoods but on groups of blocks drawn from different image locations and collected on the basis of their similarity, in the spirit of the nonlocal approach. Therefore, the resulting 3-D groups are highly redundant, allowing for a sparser WT representation and a more effective separation between signal and noise through hard thresholding in the first step; as a further consequence, statistics can be more reliably estimated, and the Wiener filtering of the second step (always working on the 3-D groups) turns out to be extremely effective.

We can now summarize, at a very high level, the processing flow of BM3-D. The first step, operating on the noisy image, comprises three stages.

1) Grouping: For each reference block, the most similar blocks are located in the image according to a minimum Euclidean distance criterion.
2) Collaborative filtering: Each 3-D group undergoes WT, hard thresholding, and inverse WT.
3) Aggregation: All filtered blocks are returned to their original location and contribute with suitable weights to the basic estimate of the image.

The second step comprises the same three stages, with the following differences.

1) Grouping: Blocks are located based on the basic estimate provided by the first step.
2) Collaborative filtering: Each 3-D group (of noisy blocks) undergoes DCT/WT, *Wiener filtering*, and inverse transform.
3) Aggregation: Like in step one.

This minimal summary is meant as a key for going through the rest of this paper. A detailed description of BM3-D, however important for a full understanding of the proposed algorithm, goes outside the scope of this work, and the reader is referred to [26] for more details.

B. Adapting BM3-D to Deal With SAR Speckle

BM3-D was developed in AWGN hypotheses, and using it with SAR images, characterized by multiplicative noise, makes little or no sense. Of course, one can always resort to the homomorphic approach, converting the multiplicative noise to additive, and using BM3-D on the transformed data, before going back to the original domain. Indeed, this simple approach provides sometimes surprisingly good results, as shown in the experimental section.[2] Nonetheless, the log-transform modifies the dynamics of the data, introducing unwanted artifacts, and the noise remains markedly non-Gaussian (particularly for the single-look case) with a sure loss of performance. Therefore, in this work, we decided to use the BM3-D filtering structure because of its compelling rationale, but also to adapt it to the specific characteristics of the data, modifying the various processing steps so as to take into account the actual statistics of SAR noise. To this end, we introduce two major modifications.

First of all, we adapt the criterion used to collect blocks in the 3-D groups to the actual data statistics. For each reference block, BM3-D looks (in a suitable search area) for those blocks which are closest to the reference in terms of Euclidean distance. In the AWGN setting, this makes perfect sense because a smaller Euclidean distance corresponds to a higher likelihood that the two signal blocks (without noise) be equal, which is what the collaborative filtering needs. However, once the noise statistics change, as what happens with SAR images, the Euclidean distance loses its significance, and we need a different *ad hoc* similarity measure in order to keep identifying the signal blocks that are more likely to be equal to the reference one.

Our second modification stems from the same line of reasoning and concerns the collaborative filtering itself. In fact, hard thresholding is a reasonable choice in AWGN, since it is the minimax estimator of the uncorrupted group [33], but this is no longer true with multiplicative noise where a more suitable wavelet shrinkage strategy can be devised. In this paper, in particular, we adopt the LLMMSE solution, discussed in depth in the next section. Together with this "compelling" modification, we introduce a further change consisting in the use of the undecimated discrete WT (UDWT), aimed at obtaining more reliable estimates in the first step, particularly needed in the presence of such intense noise. Indeed, by eliminating the decimation step, UDWT guarantees shift invariance (thus avoiding artifacts such as Gibbs phenomena after thresholding) and provides a larger number of samples for subsequent estimates. On the other hand, UDWT is quite data intensive and gives rise to correlated coefficients, thus uncoupling optimality in the original and transform domain. Nonetheless, it has been shown experimentally [38], and justified theoretically [39], to provide better results than nonredundant WT and has already been successfully applied to LLMMSE shrinkage in the case of speckle [20], [40].

III. Proposed SAR-Oriented Modifications in Detail

In this section, we analyze in some depth the modifications adopted in BM3-D in order to deal effectively with speckled SAR images. Under the hypothesis of fully developed speckle, the observed backscattered signal $z(s)$[3] can be expressed as

$$z(s) = x(s)u(s) \tag{1}$$

where $x(s)$ is the noise-free reflectance and $u(s)$ is the speckle, in intensity format, characterized by a unitary mean and independent of x. Equation (1) can be rewritten in terms of signal plus signal-dependent additive noise $v(s)$

$$\begin{aligned} z(s) &= x(s) + [u(s) - 1]\, x(s) \\ &= x(s) + u'(s)x(s) = x(s) + v(s). \end{aligned} \tag{2}$$

It is worth noting that, due to the independence of x and u, and the fact that u' has zero mean, the additive noise v, whose variance depends on x, is zero mean and appears to be uncorrelated with x. In the following, starting from the aforementioned model, and with further assumptions that both signal

[2] A more sophisticated log-domain version of BM3-D has been recently proposed in [37], which however addresses only the case of single-look amplitude images.

[3] For notational compactness, we use a single argument to indicate spatial location.

and noise are spatially uncorrelated, we will first introduce two new similarity measures and then two LLMMSE shrinkages in the transform domain, respectively, for the two steps of the algorithm.

A. Block Similarity Measure

The nonlocal approach can be regarded as an attempt (limited by complexity and data scarcity) to carry out truly statistic, as opposed to spatial, averages. Assuming one is able to collect an arbitrary number of blocks with the same signal component and differing only in the noise realization, one can easily remove most noise (all of it in the limit) with simple filtering operations. Therefore, the block-matching phase of BM3-D aims at locating the blocks most likely to have the same signal component as the reference which, in AWGN hypotheses, coincide with those having the smallest Euclidean distance from the reference in the data space.

Outside of the AWGN realm, the Euclidean distance is not optimal anymore, but one can follow the same probabilistic principle to devise a new similarity measure based on the actual noise distribution. This is done, for example, in [41] and [30] where a function of the fluctuations in the image is used, which represents the likelihood that two observations correspond to the same noise-free scene radiance.

Mathematically, given two observed amplitude values $a(s)$ and $a(t)$, with $a(\cdot) = \sqrt{z(\cdot)}$, it results in

$$p\left[a(s), a(t) | x(s) = x(t)\right] = \int_D p\left[a(s) | x(s) = \alpha\right] p\left[a(t) | x(t) = \alpha\right] p(\alpha) d\alpha \quad (3)$$

where $x(s)$ and $x(t)$ are the corresponding values of the noise-free signal, defined over the domain D, and $p(\cdot)$ indicates a probability density function. We have assumed $a(s)$ and $a(t)$ to be conditionally independent given x. This expression further simplifies to

$$p\left[a(s), a(t) | x(s) = x(t)\right] \propto \int_D p\left[a(s) | x(s) = \alpha\right] p\left[a(t) | x(t) = \alpha\right] d\alpha \quad (4)$$

if we assume, lacking any prior knowledge, $p(\cdot)$ to be uniform over D.

Considering that, for an L-look amplitude, SAR image speckle can be modeled [1], [42] by a square-root gamma distribution with order L

$$p(a|x) = \frac{2}{\Gamma(L)} \left(\frac{L}{x}\right)^L a^{2L-1} \exp\left(-L\frac{a^2}{x}\right), \qquad a \geq 0 \quad (5)$$

(4) reads as

$$p\left[a(s), a(t) | x(s) = x(t)\right] \propto \int_0^\infty \frac{4L^{2L}}{\Gamma^2(L)\alpha^{2L}} \left[a(s)a(t)\right]^{2L-1} \times \exp\left\{-\frac{L}{\alpha}\left[a^2(s) + a^2(t)\right]\right\} d\alpha \quad (6)$$

with the integral equal to [30]

$$4L\frac{\Gamma(2L-1)}{\Gamma^2(L)} \left[\frac{a(s)a(t)}{a^2(s) + a^2(t)}\right]^{2L-1}. \quad (7)$$

To translate this result into a manageable block similarity measure, we must rewrite (3) with vectors drawn from the blocks B_s and B_t in place of scalars and assume again the conditional independence of the observed values given the noise-free signal. Then, we define the block similarity measure as

$$\begin{aligned} &d\left[a(B_s), a(B_t)\right] \\ &\quad = -\log\left\{\prod_k p\left[a(s+k), a(t+k) | x(s+k) = x(t+k)\right]\right\} \\ &\quad = -\log\left\{\prod_k 4L\frac{\Gamma(2L-1)}{\Gamma^2(L)} \times \left[\frac{a(s+k)a(t+k)}{a^2(s+k) + a^2(t+k)}\right]^{2L-1}\right\} \end{aligned} \quad (8)$$

where $a(B_s)$ is the vector of observed values drawn from block B_s, s is the reference pixel of the block, and k is used to scan the whole block. Finally, discarding the constant term, the block similarity measure reduces to [30]

$$d_1\left[a(B_s), a(B_t)\right] = (2L-1)\sum_k \log\left[\frac{a(s+k)}{a(t+k)} + \frac{a(t+k)}{a(s+k)}\right] \quad (9)$$

where the subscript 1 indicates that this measure is used in the first step.

In the second step, in fact, the similarity measure must take into account the additional information provided by the first step, which is a coarse estimate of the noiseless signal $\hat{x}$. Therefore, inspired by the study in [30], where this approach is used for iterative denoising in a Bayesian framework, we define the similarity measure in the second step as

$$d_2\left[a(B_s), a(B_t)\right] = \sum_k \left[(2L-1)\log\left(\frac{a(s+k)}{a(t+k)} + \frac{a(t+k)}{a(s+k)}\right) + \gamma L \frac{\left|\hat{x}(s+k) - \hat{x}(t+k)\right|^2}{\hat{x}(s+k)\hat{x}(t+k)}\right] \quad (10)$$

where γ weighs the relative importance of the data and (loosely speaking) prior terms. Note that, unlike in [30], there is only one weight to tune, because we are only interested in ranking the blocks based on their similarity with the reference and not in computing any *absolute* measure.

B. Group Shrinkage

The hard thresholding used by BM3-D in the first step is a reasonable choice in the AWGN context, but not anymore in the presence of SAR speckle. Therefore, we address the shrinkage problem in the framework of statistical estimation, with the noise model of (2), and look for the optimum linear

estimator in the MMSE sense. It is worth emphasizing that WT and shrinkage take place on each 3-D group individually, and hence, in this section, the group will be our basic data unit. After the linear WT, we obtain

$$\mathbf{Z} = \mathbf{X} + \mathbf{V} \tag{11}$$

where we have used capital letters for the transformed data and boldface to indicate the vectors formed by all the coefficients of the group. Under the constraint of linearity, the optimal MMSE estimator is [43]

$$\hat{\mathbf{X}} = E[\mathbf{X}] + (\mathbf{C}_{XZ})(\mathbf{C}_Z)^{-1}(\mathbf{Z} - E[\mathbf{Z}]) \tag{12}$$

where $E[\cdot]$ denotes statistical expectation, $\mathbf{C}_Z$ is the covariance matrix of $\mathbf{Z}$, and $\mathbf{C}_{XZ}$ is the cross-covariance matrix of $\mathbf{X}$ and $\mathbf{Z}$. Since signal and noise are uncorrelated in the spatial domain, they remain uncorrelated also after the linear transform, with noise still zero mean; therefore, (12) simplifies to [43]

$$\hat{\mathbf{X}} = E[\mathbf{X}] + (\mathbf{C}_X)(\mathbf{C}_X + \mathbf{C}_V)^{-1}(\mathbf{Z} - E[\mathbf{Z}])\,. \tag{13}$$

If we further assume that the covariance matrices are diagonal, the estimation acts separately on each coefficient of the group

$$\hat{X}(i) = E[X(i)] + \frac{\sigma_X^2(i)}{\sigma_X^2(i) + \sigma_V^2(i)}(Z(i) - E[Z(i)]) \tag{14}$$

and we obtain an LLMMSE filter, which is, indeed, an adaptive Wiener filter in the transform domain [19], [44].

The hypothesis that both signal and noise coefficients are uncorrelated is quite reasonable when a WT is used, since it tends to decorrelate the data, and in fact, the local Wiener filter has been used extensively in the AWGN context [34], [45]–[47] providing a performance typically superior to that of classical thresholding. Of course, such hypothesis does not hold anymore with the UDWT, which is nonorthogonal and introduces some redundancy among the coefficients. Nonetheless, even in this case, such an assumption is typically convenient, as the cost for the imperfect modeling is more than compensated by the opportunity to use a local estimator and by the significant reduction in complexity.

Since the shrinkage is applied only to the coefficients of the detail subbands, which can be reasonably considered to have zero mean, (14) eventually becomes

$$\hat{X}(i) = \frac{E\left[X^2(i)\right]}{E\left[X^2(i)\right] + E\left[V^2(i)\right]} Z(i) \tag{15}$$

or equivalently

$$\hat{X}(i) = \frac{E\left[Z^2(i)\right] - E\left[V^2(i)\right]}{E\left[Z^2(i)\right]} Z(i). \tag{16}$$

The problem now comes down to the estimation of the second-order moments in the aforementioned formulas. In the literature, working with large images, these quantities are typically computed by means of sliding-window averages running on the various detail subbands of the WT. In our case, however, we deal with rather small groups (e.g., $8 \times 8 \times 16$ coefficients) which, after an ordinary WT, would be decomposed in tiny detail subbands, making any such estimate totally unreliable. This is why we turn to UDWT for the first shrinkage step, as it provides us with subbands large enough to carry out reliable estimates.

1) *First step*: To carry out the estimates required in (16), we assume that the second-order statistics of the observed signal, given the limited size of the 3-D group, are constant over the whole group in the spatial domain, and over each subband in the transform domain. Therefore, we have

$$E\left[Z^2(i)\right] = \langle Z^2 \rangle_{SB(i)} = \frac{1}{|SB(i)|} \sum_{j \in SB(i)} Z^2(j) \tag{17}$$

where $\langle \cdot \rangle_{SB(i)}$ indicates the average over the subband comprising the ith coefficient.

As for the noise, this problem was addressed in [20] with reference to the UDWT case, obtaining

$$E\left[V^2(i)\right] = \frac{\sigma_u^2}{(1+\sigma_u^2)} \sum_k h^2(k) E\left[z^2(i-k)\right] \tag{18}$$

where h is the subband equivalent filter, σ_u^2 is a known parameter depending on speckle format and number of looks [42], and k spans a 7×7 local window. Adapting the formula to our case, we readily obtain

$$E\left[V^2(i)\right] = \frac{\sigma_u^2}{(1+\sigma_u^2)} \langle z^2 \rangle_G \tag{19}$$

where $\langle \cdot \rangle_G$ indicates the average over the whole group. It is worth observing that the increase in complexity due to the use of an undecimated transform is compensated by the use of subband-wise and group-wise, as opposed to sliding-window averages.

Eventually, we have

$$\hat{X}_1(i) = \max\left(0, \frac{\langle Z^2 \rangle_{SB(i)} - \frac{\sigma_u^2}{(1+\sigma_u^2)} \langle z^2 \rangle_G}{\langle Z^2 \rangle_{SB(i)}}\right) Z(i) \tag{20}$$

where the subscript 1 indicates first step and the max operator accounts for a possible sign inversion due to estimation errors.

2) *Second step*: The collaborative filtering in the second step also has an LLMMSE nature with the major difference that now an estimate of the noiseless signal coefficient is already available. As a first consequence, we can use simpler nonredundant transforms, thus reducing complexity. In addition, with reference to (15), we estimate $E[X^2(i)]$ simply as $\hat{X}_1^2(i)$, where $\hat{X}_1(i)$ is the coefficient computed from the partially denoised signal $\hat{x}_1(n)$ provided by the first step. This amounts to using the empirical Wiener filtering, proposed in [34] for the AWGN context and also used in the original BM3-D [26]. Finally, to estimate $E[V^2(i)]$, we assume that it is constant over the group and exploit again the first-step estimate $\hat{X}_1^2(i)$ carrying out an

average over the whole group of the difference between the observed coefficient and its noiseless estimate as

$$E\left[V^2(i)\right] = \langle V^2 \rangle_G = \frac{1}{|G|} \sum_{i \in G} \left[Z(i) - \hat{X}_1(i) \right]^2. \quad (21)$$

In conclusion, the second-step estimate reads

$$\hat{X}_2(i) = \frac{\hat{X}_1^2(i)}{\hat{X}_1^2(i) + \langle V^2 \rangle_G} Z(i). \quad (22)$$

C. Aggregation

To conclude the description of our algorithm, let us focus on the aggregation phase. Since a given pixel $x(s)$ can be included in more than one group, and hence estimated several times, each time with a possibly different value, such values must be averaged using suitable weights

$$\hat{x}(s) = \frac{1}{T} \sum_{G \in \mathcal{G}(s)} w_G \hat{x}_G(s). \quad (23)$$

Here, $\hat{x}_G(s)$ is the estimate provided from group G through inverse transform, w_G is the corresponding weight, $\mathcal{G}(s)$ is the set of all groups comprising $x(s)$, and $T = \sum_{G \in \mathcal{G}(s)} w_G$ is a normalizing factor.

Like in [26], the weights are made to depend on the presumed reliability of the associated group estimate, related in turn to the average noise power of the group after shrinkage. In formulas

$$w_G \propto \frac{1}{\langle V^2 \rangle_G \langle S^2(i) \rangle_G} \quad (24)$$

where $S(i)$ is the shrinkage factor for the ith coefficient of the group. Both (23) and (24) hold for both steps (we put no subscripts to simplify notation), although the expressions for $\langle V^2 \rangle_G$ and for the shrinkage factors are obviously different.

IV. Experimental Results

In SAR image denoising, given the lack of the original noiseless signal, performance assessment is quite a challenging task. Different indicators have been proposed to measure smoothness of smooth areas as well as sharpness of edges and details, but they are largely empirical and provide little insight about how to balance image cleanness and preservation of diagnostic information. Therefore, following an approach widespread in the literature [18], [20], [21], [30], we start with experiments carried out on optical images corrupted by simulated speckle, obtaining objective performance figures which allow a sound comparison among different denoising algorithms. Then, in Section IV-C, we discuss experiments with actual SAR images.

A. Reference Techniques and Parameter Setting

We compare the proposed technique with three state-of-the-art despeckling algorithms: The spatially adaptive wavelet homomorphic shrinkage algorithm (SA-WBMMAE) [18], the wavelet-based MAP filtering algorithm (MAP-S) [22], and the PPB nonlocal filter [30].

Such techniques have been chosen because of their competitive performance and (not least) for the availability of software code to run the experiments. Experimental results have, in fact, been obtained by using the authors' own code available online or run by the authors themselves on our test images. We also include in the comparison two state-of-the-art AWGN techniques used in a homomorphic setting (with mean-bias correction), the AWGN versions of PPB (H-PPB) and BM3-D (H-BM3-D), which are particularly interesting for images with a large number of looks. Finally, we also consider the well-known Frost filter [7] which, although pretty aged, is a *de facto* standard, included in many image processing software packages, and used routinely by photo interpreters of military and civil space agencies.

For all these algorithms, if not stated otherwise, the free parameters are set as suggested in the reference papers. As for the proposed SAR-BM3-D algorithm, in the first step, we use a Daubechies-8 UDWT transform with a three-level decomposition, and fixed groups of dimension $8 \times 8 \times 16$. Just like in BM3-D, the computational burden is reduced by using a relatively small search area, 39×39, and by selecting reference blocks only on every third row and column. Similar choices apply to the second step except for the transform, which is a spatial DCT followed by a Haar DWT along the blocks with a maximum-level decomposition, and for the group dimensions that grow to $8 \times 8 \times 32$. Finally, the weight γ in the similarity measure of (10) was set equal to one, which was found experimentally to guarantee a good performance.

B. Results With Simulated Speckle

In order to obtain reliable results, we considered a variety of sources, including some general-purpose images commonly used in the AWGN denoising literature, some aerial photographs which better resemble SAR images in terms of scene structure, and a synthetic image, first introduced by Lee in [48], in order to test structure preservation. SAR-like images are obtained by multiplying optical images by simulated white speckle in amplitude format (square-root intensity model) [42] with pdfs corresponding to the cases of 1, 2, 4, and 16 looks. All numerical results are obtained as the average over ten different realizations of the noise process.

The performance is quantified by the peak signal-to-noise ratio (PSNR)

$$PSNR = 10 \log_{10} \frac{|x|^2_{\max}}{MSE} \quad (25)$$

where $|x|_{\max}$ is the maximum value admitted by the data format and the mean-square error

$$MSE = \left\langle \left[x(n) - \hat{x}(n) \right]^2 \right\rangle \quad (26)$$

is computed as a spatial average $\langle \cdot \rangle$, with x and $\hat{x}$ being the original and denoised images, respectively.

In Table I, we report the results for two[4] general-purpose 512×512-pixel images, Lena and Boat (Fig. 1), widely used

[4]Numerical results for *all* tested images, as well as all original and denoised versions of the images, are available at http://www.dibet.unina.it/grip/downloads/tgrs11_additional_material.zip.

TABLE I
PSNR RESULTS FOR LENA, BOAT, AND NAPOLI

	Lena				Boat				Napoli			
	L=1	L=2	L=4	L=16	L=1	L=2	L=4	L=16	L=1	L=2	L=4	L=16
Noisy	12.11	14.89	17.80	23.76	11.77	14.55	17.46	23.42	14.29	17.07	19.98	25.94
Frost	19.17	23.31	26.33	30.59	18.65	22.58	25.22	28.33	20.36	23.52	25.16	26.41
SA-WBMMAE	25.06	27.26	29.04	32.40	23.29	25.22	26.84	29.94	22.09	23.42	24.79	27.73
MAP-S	26.35	28.04	29.78	33.19	23.98	25.43	27.05	30.48	22.09	23.45	25.03	29.09
PPB	26.71	28.44	29.84	32.68	24.01	25.59	26.96	29.83	21.37	22.64	24.34	28.14
SAR-BM3D	**27.93**	**29.62**	31.21	34.15	**25.50**	**26.94**	28.44	31.43	**23.56**	**25.02**	**26.63**	**30.09**
H-PPB	25.26	27.83	29.68	32.86	23.40	25.41	27.00	29.97	19.61	22.13	24.42	28.49
H-BM3D	26.40	29.18	**31.23**	**34.51**	24.49	26.75	**28.58**	**31.74**	22.92	24.69	26.37	29.96

(a) (b) (c)

Fig. 1. Original images used in the experiments. (a) Lena. (b) Boat. (c) Napoli.

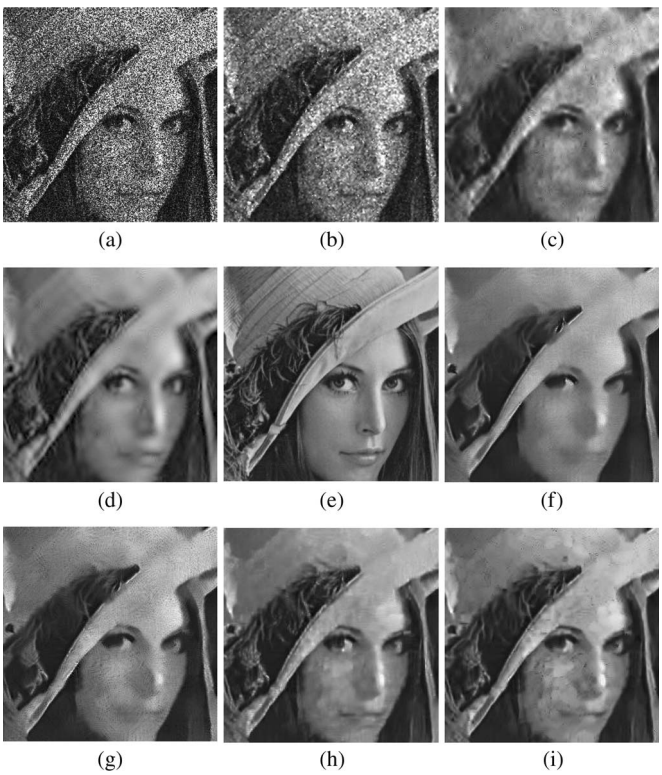

(a) (b) (c)

(d) (e) (f)

(g) (h) (i)

Fig. 2. Zoom of filtered images for Lena corrupted by one-look speckle. (a) Noisy image. (b) Frost. (c) SA-WBMMAE. (d) MAP-S. (e) Original image. (f) PPB. (g) H-PPB. (h) SAR-BM3-D. (i) H-BM3-D.

as benchmark in the denoising community, for $L = 1, 2, 4$, and 16 looks. The best PSNR for each case is put in boldface for the sake of clarity. Although the Frost filter does already a good job, with an improvement of several decibels w.r.t. the noisy image, more sophisticated techniques prove definitely superior, particularly for the most critical case of $L = 1$ (no multilook), where an additional gain of 6–8 dB is achieved. SAR-BM3-D provides consistently the best performance, gaining from 1 to 1.5 dB w.r.t. PPB which looks as the second best. The only exception to this rule is represented by the homomorphic version of BM3-D (H-BM3-D) which, for large L, is slightly superior even to the proposed dedicated technique. As a matter of fact, the two algorithms based on the homomorphic approach exhibit quite a similar behavior, becoming more and more competitive with increasing L. This is not surprising, however, since the noise in the log image tends to become Gaussian as L increases, in which case a general-purpose AWGN denoising algorithm in the homomorphic setting becomes a perfectly sensible choice. In the absence of multilook, instead, the proposed SAR-dedicated algorithm provides a clear advantage over the homomorphic approach. Fig. 2 shows the zoom of the denoised images provided by all algorithms for Lena with $L = 1$. It is clear that strong noise reduction comes at the price, in general, of some loss of details, most notable in the PPB image. SAR-BM3-D and H-BM3-D seem to offer the best compromise between these contrasting needs, but the latter also introduces a number of pointwise artifacts which severely degrade the image quality.

Table I gives also results for a 512×512-pixel section of an aerial photo showing a prevalently urban scene in the city of Naples (Italy) (Fig. 1). The general behavior of the PSNR is quite similar to that of the previous experiments, except for the gap between SAR-BM3-D and the reference techniques which grows slightly larger. It is worth taking a closer look, instead, at the zoom of denoised images shown in Fig. 3. Here, given the wealth of fine details in the original image, the smoothing provided by some filtering techniques is particularly annoying, with many individual objects, both cars and boats, merged together or even lost in the background. SAR-BM3-D, instead, and, to a lesser extent, H-BM3-D and PPB (with a modified setting proposed by the authors) provide an acceptable balance between smoothing and detail preservation. The latter two, however, introduce again very visible and annoying artifacts.

To better substantiate this claim, Table II provides results in terms of the edge-preservation index β proposed in [16], obtained as the correlation coefficient between the high-pass versions of original and filtered images. Even though this index is largely empirical, and hence should be considered with some reservation, it speaks very clearly in favor of SAR-BM3-D and H-BM3-D, with all other techniques, including both versions of PPB, lagging far behind.[5]

[5]Similar results, with minor variations, are obtained with all the images; they are not reported in this paper to save space.

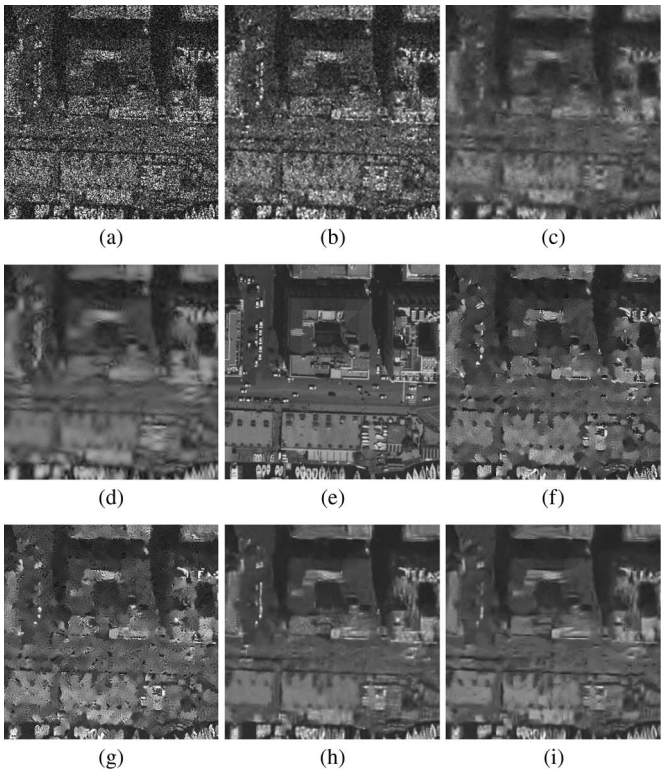

Fig. 3. Zoom of filtered images for Napoli corrupted by one-look speckle. (a) Noisy image. (b) Frost. (c) SA-WBMMAE. (d) MAP-S. (e) Original image. (f) PPB. (g) H-PPB. (h) SAR-BM3-D. (i) H-BM3-D.

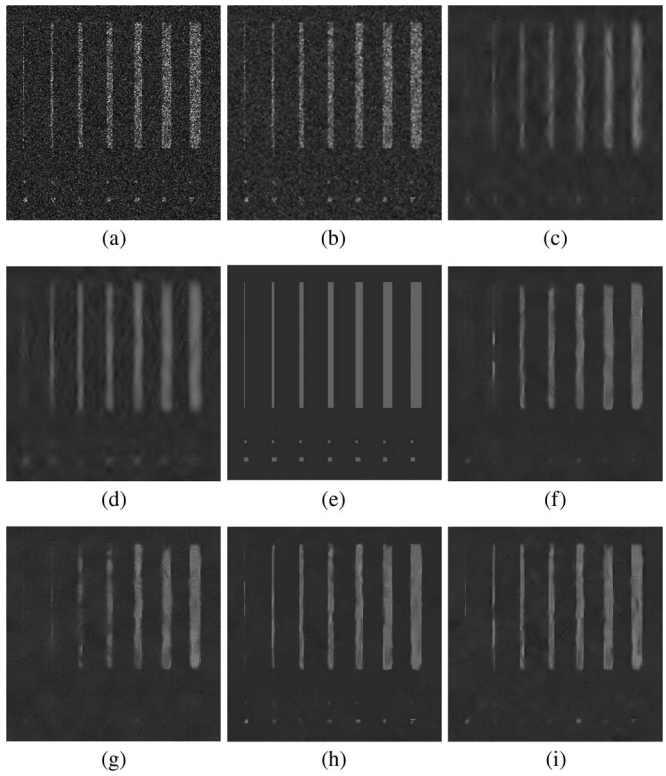

Fig. 4. Filtered images for target corrupted by one-look speckle. (a) Noisy image. (b) Frost. (c) SA-WBMMAE. (d) MAP-S. (e) Original image. (f) PPB. (g) H-PPB. (h) SAR-BM3-D. (i) H-BM3-D.

TABLE II
β INDEX FOR NAPOLI

	L=1	L=2	L=4	L=16
Noisy	0.259	0.360	0.484	0.744
Frost	0.350	0.463	0.505	0.517
SA-WBMMAE	0.346	0.465	0.559	0.745
MAP-S	0.287	0.392	0.536	0.820
PPB	0.340	0.468	0.594	0.788
SAR-BM3D	**0.487**	**0.603**	**0.706**	**0.857**
H-PPB	0.285	0.450	0.599	0.801
H-BM3D	0.445	0.590	0.698	0.855

TABLE III
PSNR AND DETECTION RESULTS FOR TARGET. DETECTION RESULTS ARE IN TERMS OF AVERAGE NUMBER OF IDENTIFIED FEATURES (OVER TEN REALIZATIONS) OF THE SINGLE-LOOK IMAGE

	L=1	L=2	L=4	L=16	bars	5×5	3×3	1×1	F.A.
Noisy	17.68	20.48	23.39	29.34	–	–	–	–	–
Frost	24.39	28.15	30.44	32.71	6.8	7	7	3.7	~ 100
SA-WBMMAE	28.20	29.75	31.13	35.06	6.0	7	1.4	0.2	~ 10
MAP-S	28.95	30.31	32.00	36.89	6.7	6.8	2.4	0.5	~ 10
PPB	30.06	32.74	35.48	40.31	5.6	3.4	0	0	0
SAR-BM3D	**32.51**	**36.30**	**39.80**	**45.67**	6.2	7	2.9	0	0
H-PPB	28.07	31.33	34.47	39.58	5.3	2.4	0	0	0
H-BM3D	30.79	35.23	38.59	45.05	6.3	4.6	1.0	0	~ 10

Table III finally presents results for the synthetic 256 × 256-pixel target image, reported for the first time in [48], which contains points and strips of increasing dimensions. The point targets have size of 1 × 1, 3 × 3, and 5 × 5 pixels, while the strip width goes from 1 to 13 pixels in 2-pixel increments. All target pixels have value 120, while the background pixels have value 60. In terms of PSNR, the most significant difference w.r.t. previous experiments is the larger gain of the BM3-D-based techniques over the others. This is probably due to the block-wise processing used in BM3-D, which allows one to treat coherently neighboring pixels. Filtered images are shown in Fig. 4. To test feature preservation, we decided to process them with a simple detector (a Gaussian filter followed by a threshold operator), declaring the detection of a target whenever an above-threshold region superimposed the target. Results, in terms of the number of detected features (over ten realizations) in the single-look case, are reported again in Table III and confirm what visual inspection also suggests, namely, that all filters behave about equally well on point targets (lost) and bars (saved), but only SAR-BM3-D and Frost save all 5 × 5 and quite a few 3 × 3 targets, with the latter generating however an inordinate amount of false alarms (F.A.).

C. Results With Actual SAR Images

For this set of experiments, we considered five single-look and one 6-look TerraSAR-X images in amplitude format taken over Rosenheim (Rs) in Germany and Toronto (Tr) in Canada. Fig. 5 shows 512 × 512-pixel sections drawn from such images covering heterogeneous sceneries: urban areas, fields, woods, and a lake. For these images, we computed the equivalent number of looks (ENL), a standard parameter widely used in the remote sensing community which measures the speckle reduction in homogeneous areas. Once an apparently homogeneous region in the image is selected, like those in the white boxes in Fig. 5, the ENL is computed as

$$ENL = \mu_{\hat{x}}^2/\sigma_{\hat{x}}^2 \tag{27}$$

with $\mu_{\hat{x}}^2$ being the average intensity of the selected area and $\sigma_{\hat{x}}^2$ as its variance. Larger ENL values indicate stronger speckle

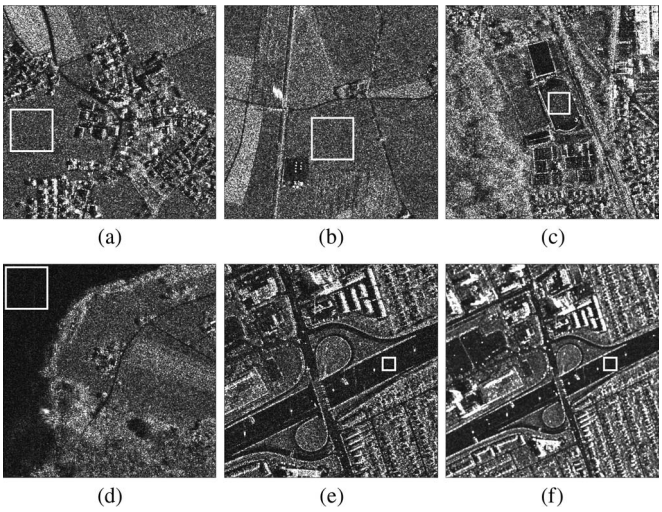

Fig. 5. Test SAR-X images (Infoterra GmbH) with selected areas for ENL computation (white box). (a) Rs 1, $L = 1$. (b) Rs 2, $L = 1$. (c) Rs 3, $L = 1$. (d) Rs 4, $L = 1$. (e) Tr, $L = 1$. (f) Tr, $L = 6$.

TABLE IV
ENL FOR REAL SAR IMAGES

	Rs 1	*Rs 2*	*Rs 3*	*Rs 4*	*Tr L1*	*Tr L6*
Noisy	0.95	0.98	0.90	0.94	0.91	7.43
Frost	3.57	3.80	3.05	3.71	3.39	14.66
SA-WBMMAE	3.08	3.05	2.36	2.29	2.79	9.63
MAP-S	14.55	18.56	5.73	18.56	6.70	12.86
PPB	43.01	47.04	19.79	51.24	66.59	15.35
SAR-BM3D	6.75	8.03	4.84	7.78	7.76	11.99
H-BM3D	3.62	3.27	2.76	3.16	3.79	8.58
H-PPB	6.56	4.37	3.85	3.56	7.48	8.89

rejection and, consequently, an improved ability to tell apart different gray levels. Table IV reports the ENL values for the proposed and reference algorithms.

Results are quite consistent, indicating PPB[6] by far as the technique with the strongest speckle rejection ability, followed by H-PPB, MAP-S, SAR-BM3-D, and the others. On the other hand, this is immediately obvious by visual inspection of results, like those for the Rosenheim 3 image[7] whose filtered versions are shown in Fig. 6. Although the PPB image looks more pleasant than the others and is probably more helpful to gain a quick insight of the scene, it presents widespread artifacts resembling watercolor strokes. Indeed, SAR-BM3-D seems to be the only technique which guarantees a significant noise reduction without introducing some kinds of artifacts. However, with neither the noiseless image nor an expert interpreter, it is difficult to decide whether such artifacts imply any loss of details. Some help comes from the analysis of ratio images obtained, as proposed in [1], as the pointwise ratio between the SAR original z and denoised $\hat{x}$ images

$$R = z/\hat{x}. \tag{28}$$

Given a perfect denoising, i.e., $\hat{x} = x$, the ratio image should contain only speckle, possibly with the expected statistics. On the contrary, the presence of geometric structures or details

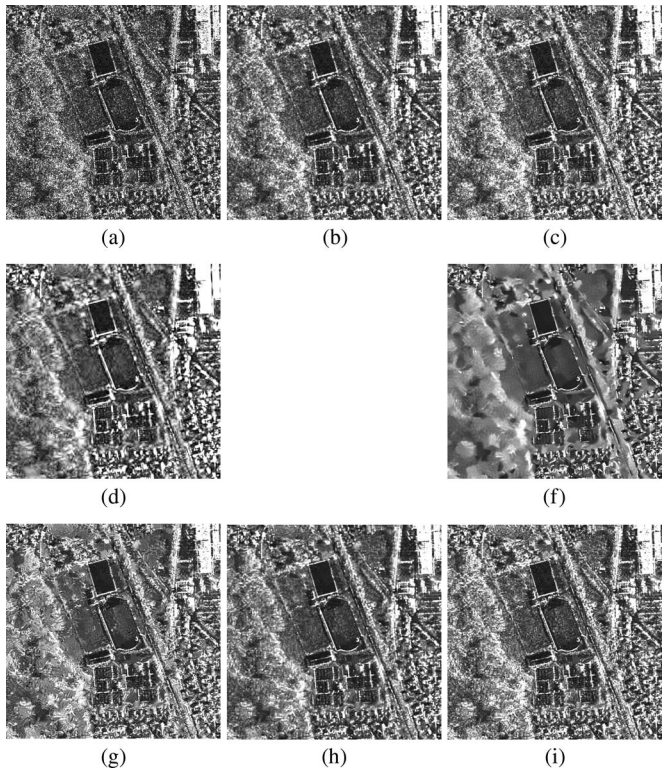

Fig. 6. Filtered images for Rs 3. (a) SAR image. (b) Frost. (c) SA-WBMMAE. (d) MAP-S. (f) PPB. (g) H-PPB. (h) SAR-BM3-D. (i) H-BM3-D.

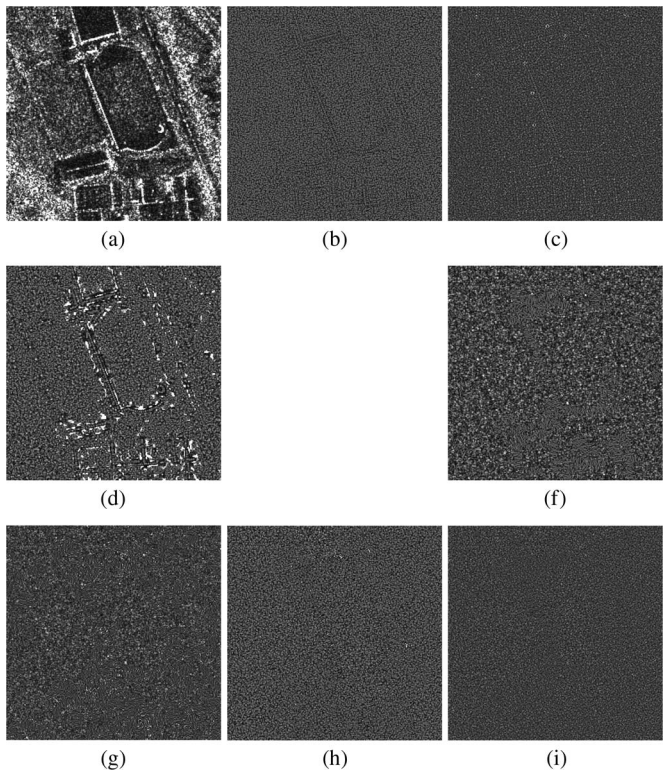

Fig. 7. Zoom of enhanced ratio between the noisy and denoised images. (a) SAR image. (b) Frost. (c) SA-WBMMAE. (d) MAP-S. (f) PPB. (g) H-PPB. (h) SAR-BM3-D. (i) H-BM3-D.

correlated to the original image indicates that the algorithm has removed not only noise but also some information of interest. Fig. 7 shows the amplitude ratio images, scaled by

[6]In the case $L = 6$ (low-resolution images), the parameter setting is the same, used for Naples as indicated by the authors.

[7]Again, detailed results for all images are available at http://www.dibet.unina.it/grip/downloads/tgrs11_additional_material.zip.

a factor 100 corresponding to the denoised images in Fig. 6. The Frost ratio image presents visible traces of the man-made structures, denouncing an unwanted smoothing of sharp boundaries, and similar traces, although weaker, are also present for SA-WBMMAE and MAP-S. The PPB and H-PPB ratio images exhibit different patterns depending on the different areas of the scene, although not marked by linear structures, showing again a dependence on the original SAR image. In SAR-BM3-D and H-BM3-D ratio images, finally, there is no trace of man-made structures nor any obvious pattern.

Regarding the ratio statistics, the expected value is often used in the SAR literature to test the level of bias introduced by the denoising process. Since the considered techniques are designed to preserve the mean of backscattered intensity, the expected value of intensity ratio should be equal to one [1]. The considered algorithms exhibit averages from a minimum of about 0.75 for homomorphic methods through 0.89 for SAR-BM3-D, to a maximum of 0.92 for PPB. Small values indicate a tendency to "follow" the noise, and hence perform a lighter filtering, but all observed values are reasonably large. Very likely, this is a consequence of the speckle affecting TerraSAR-X images, which does not match the hypotheses of the theoretical model. Indeed, no such polarization is observed in the simulated images for any considered algorithm.

V. Conclusion and Future Work

In this paper, we have proposed a novel and very promising algorithm for SAR image despeckling. We have drawn concepts and tools from the nonlocal filtering approach, adapting them to the specificities of SAR imagery. Major innovations regard the choice of the similarity measure, which takes into account the probabilistic noise distribution of speckle, and the wavelet shrinkage in the 3-D domain, which is derived from the additive signal-dependent model following a linear MMSE estimation approach.

Results on simulated speckled images are quite satisfactory, with a consistent PSNR gain of 1–2 dB over the best reference algorithms to date. Similar improvements are observed in a simple automatic detection task on a synthetic image. Experiments on actual SAR images are likewise encouraging, as the proposed technique seems to have a better capacity to preserve relevant details while smoothing homogeneous areas.

There are several aspects of the proposed algorithm that can be improved. In particular, the speckle statistics of actual SAR images, particularly at high resolution, often deviate from the simplified model used in this work, as well as in most of the literature, explaining the different performance observed on simulated and real SAR images. Adapting the algorithm to the case of correlated speckle will be certainly the object of future work.

Another sore point is the lack of objective quality measure for SAR images which weakens all experimental analyses. We are therefore set to carry out a more thorough and reliable analysis of SAR despeckling algorithms, based on *ad hoc* simulated SAR images and indicators, as well as on the measurable performance of algorithms and human interpreters on a large set of denoised images.

Acknowledgment

The authors would like to thank T. Bianchi for processing data with the MAP-S filter and M. I. H. Bhuiyan for providing SA-WMMAE code. The authors would also like to thank Prof. G. Poggi for his helpful comments and suggestions.

References

[1] C. Oliver and S. Quegan, *Understanding Synthetic Aperture Radar Images*. Raleigh, NC: SciTech, 2004.

[2] H. H. Arsenault and M. Levesque, "Combined homomorphic and local-statistics processing for restoration of images degraded by signal-dependent noise," *Appl. Opt.*, vol. 23, no. 6, pp. 845–850, Mar. 1984.

[3] P. F. Yan and C. H. Chen, "An algorithm for filtering multiplicative noise in wide range," *Traitement du Signal*, vol. 3, no. 2, pp. 91–96, 1986.

[4] H. H. Arsenault and G. April, "Properties of speckle integrated with a finite aperture and logarithmically transformed," *J. Opt. Soc. Amer.*, vol. 66, no. 11, pp. 1160–1163, Nov. 1976.

[5] J. S. Lee, "Digital image enhancement and noise filtering by use of local statistics," *IEEE Trans. Pattern Anal. Mach. Intell.*, vol. PAMI-2, no. 2, pp. 165–168, Mar. 1980.

[6] J. S. Lee, "Refined filtering of image noise using local statistics," *Comput. Graph. Image Process.*, vol. 15, no. 4, pp. 380–389, Apr. 1981.

[7] V. S. Frost, J. A. Stiles, K. S. Shanmugan, and J. C. Holtzman, "A model for radar images and its application to adaptive digital filtering of multiplicative noise," *IEEE Trans. Pattern Anal. Mach. Intell.*, vol. PAMI-4, no. 2, pp. 157–166, Mar. 1982.

[8] D. T. Kuan, A. A. Sawchuk, T. C. Strand, and P. Chavel, "Adaptive noise smoothing filter for images with signal-dependent noise," *IEEE Trans. Pattern Anal. Mach. Intell.*, vol. PAMI-7, no. 2, pp. 165–177, Mar. 1985.

[9] R. Touzi, A. Lopes, and P. Bousquet, "A statistical and geometrical edge detector for SAR images," *IEEE Trans. Geosci. Remote Sens.*, vol. 26, no. 6, pp. 764–773, Nov. 1988.

[10] A. Lopes, R. Touzi, and E. Nezry, "Adaptive speckle filters and scene heterogeneity," *IEEE Trans. Geosci. Remote Sens.*, vol. 28, no. 6, pp. 992–1000, Nov. 1990.

[11] D. T. Kuan, A. A. Sawchuk, T. C. Strand, and P. Chavel, "Adaptive restoration of images with speckle," *IEEE Trans. Acoust., Speech, Signal Process.*, vol. ASSP-35, no. 3, pp. 373–383, Jan. 1987.

[12] A. Lopes, E. Nezry, R. Touzi, and H. Laur, "Maximum *a posteriori* speckle filtering and first order texture models in SAR images," in *Proc. IEEE Int. Geosci. Remote Sens. Symp.*, May 1990, vol. 3, pp. 2409–2412.

[13] E. Nezry, A. Lopes, and R. Touzi, "Detection of structural and textural features for SAR image filtering," in *Proc. IEEE Int. Geosci. Remote Sens. Symp.*, 1991, vol. 3, pp. 2169–2172.

[14] H. Guo, J. Odegard, M. Lang, R. Gopinath, L. Selesnick, and C. Burrus, "Wavelet based speckle reduction with application to SAR based ATD/R," in *Proc. IEEE Int. Conf. Image Process.*, 1994, vol. 1, pp. 75–79.

[15] L. Gagnon and A. Jouan, "Speckle filtering of SAR images: A comparative study between complex wavelet-based and standard filters," *Proc. SPIE*, vol. 3169, pp. 80–91, 1997.

[16] A. Achim, P. Tsakalides, and A. Bezarianos, "SAR image denoising via Bayesian wavelet shrinkage based on heavy-tailed modeling," *IEEE Trans. Geosci. Remote Sens.*, vol. 41, no. 8, pp. 1773–1784, Aug. 2003.

[17] S. Solbø and T. Eltoft, "Homomorphic wavelet-based statistical despeckling of SAR images," *IEEE Trans. Geosci. Remote Sens.*, vol. 42, no. 4, pp. 711–721, Apr. 2004.

[18] M. Bhuiyan, M. Ahmad, and M. Swamy, "Spatially adaptive wavelet based method using the cauchy prior for denoising the SAR images," *IEEE Trans. Circuits Syst. Video Technol.*, vol. 17, no. 4, pp. 500–507, Apr. 2007.

[19] H. Xie, L. Pierce, and F. Ulaby, "Despeckling SAR images using a low complexity wavelet denoising process," in *Proc. IEEE Int. Geosci. Remote Sens. Symp.*, Nov. 2002, vol. 1, pp. 321–324.

[20] F. Argenti and A. Alparone, "Speckle removal from SAR images in the undecimated wavelet domain," *IEEE Trans. Geosci. Remote Sens.*, vol. 40, no. 11, pp. 2363–2374, Nov. 2002.

[21] F. Argenti, T. Bianchi, and A. Alparone, "Multiresolution MAP despeckling of SAR images based on locally adaptive generalized Gaussian pdf modeling," *IEEE Trans. Image Process.*, vol. 15, no. 11, pp. 3385–3399, Nov. 2006.

[22] F. Argenti, T. Bianchi, and A. Alparone, "Segmentation-based MAP despeckling of SAR images in the undecimated wavelet domain," *IEEE Trans. Geosci. Remote Sens.*, vol. 46, no. 9, pp. 2728–2742, Sep. 2008.

[23] J. J. Ranjani and S. Thiruvengadan, "Dual-tree complex wavelet transform based SAR despeckling using interscale dependence," *IEEE Trans. Geosci. Remote Sens.*, vol. 48, no. 6, pp. 2723–2731, Jun. 2010.
[24] D. Gleich, M. Kseneman, and M. Datcu, "Despeckling of TerraSAR-X data using second-generation wavelets," *IEEE Geosci. Remote Sens. Lett.*, vol. 7, no. 1, pp. 68–72, Jan. 2010.
[25] A. Buades, B. Coll, and J. M. Morel, "A review of image denoising algorithms, with a new one," *Multiscale Model. Simul.*, vol. 4, no. 2, pp. 490–530, Jul. 2005.
[26] K. Dabov, A. Foi, V. Katkovnik, and K. Egiazarian, "Image denoising by sparse 3D transform-domain collaborative filtering," *IEEE Trans. Image Process.*, vol. 16, no. 8, pp. 2080–2095, Aug. 2007.
[27] V. Katkovnik, A. Foi, K. Egiazarian, and J. Astola, "From local kernel to nonlocal multiple-model image denoising," *Int. J. Comput. Vis.*, vol. 86, no. 1, pp. 1–30, Jan. 2010.
[28] P. Coupé, P. Hellier, C. Kervrann, and C. Barillot, "Bayesian non local means-based speckle filtering," in *Proc. 5th IEEE Int. Symp. Biomed. Imaging*, May 2008, pp. 1291–1294.
[29] H. Zhong, J. Xu, and L. Jiao, "Classification based nonlocal means despeckling for SAR image," *Proc. SPIE*, vol. 7495, p. 749 50V, Oct. 2009.
[30] C. Deledalle, L. Denis, and F. Tupin, "Iterative weighted maximum likelihood denoising with probabilistic patch-based weights," *IEEE Trans. Image Process.*, vol. 18, no. 12, pp. 2661–2672, Dec. 2009.
[31] S. Parrilli, M. Poderico, C. Angelino, G. Scarpa, and L. Verdoliva, "A nonlocal approach for SAR image denoising," in *Proc. IEEE Int. Geosci. Remote Sens. Symp.*, Jul. 2010, pp. 726–729.
[32] S. Mallat, *A Wavelet Tour of Signal Processing*. Boston, MA: Academic, 1998.
[33] D. Donoho, "De-noising by soft-thresholding," *IEEE Trans. Inf. Theory*, vol. 41, no. 3, pp. 613–627, May 1995.
[34] S. Ghael, A. Sayeed, and R. Baraniuk, "Improved wavelet denoising via empirical Wiener filtering," *Proc. SPIE*, vol. 5, pp. 389–399, Jul. 1997.
[35] A. Efros and T. Leung, "Texture synthesis by non parametric sampling," in *Proc. Int. Conf. Comput. Vis.*, 1999, vol. 2, pp. 1033–1038.
[36] L. P. Yaroslavsky, *Digital Picture Processing, an Introduction*. Berlin, Germany: Springer-Verlag, 1985.
[37] H. Mäkitalo, A. Foi, D. Fevralev, and V. Lukin, "Denoising of single-look SAR images based on variance stabilization and nonlocal filters," in *Proc. Int. Conf. MMET*, Sep. 2010, pp. 1–4.
[38] M. Lang, H. Guo, and J. E. Odegard, "Noise reduction using undecimated discrete wavelet transform," *IEEE Signal Process. Lett.*, vol. 3, no. 1, pp. 10–12, Jan. 1996.
[39] M. Elad, "Why simple shrinkage is still relevant for redundant representations?," *IEEE Trans. Inf. Theory*, vol. 52, no. 12, pp. 5559–5569, Nov. 2006.
[40] L. Zhang, P. Bao, and X. Wu, "Multiscale LMMSE-based image denoising with optimal wavelet selection," *IEEE Trans. Circuits Syst. Video Technol.*, vol. 15, no. 4, pp. 469–481, Apr. 2005.
[41] Y. Matsushita and S. Lin, "A probabilistic intensity similarity measure based on noise distributions," in *Proc. IEEE Conf. Comput. Vis. Pattern Recog.*, 2007, pp. 1–8.
[42] H. Xie, L. Pierce, and F. Ulaby, "Statistical properties of logarithmically transformed speckle," *IEEE Trans. Geosci. Remote Sens.*, vol. 40, no. 3, pp. 721–727, Mar. 2002.
[43] S. M. Kay, *Fundamentals of Statistical Signal Processing: Estimation Theory*. Englewood Cliffs, NJ: Prentice-Hall, 1993.
[44] R. Öktem and K. Egizarian, "Transform domain algorithm for reducing effect of film-grain noise in image compression," *Electron. Lett.*, vol. 35, no. 21, pp. 1830–1831, Oct. 1999.
[45] M. K. Mihcak, I. Kozintsev, and K. Ramchandran, "Spatially adaptive statistical modeling of wavelet image coefficients and its application to denoising," in *Proc. IEEE Int. Conf. Acoust., Speech, Signal Process.*, Phoenix, AZ, Mar. 1999, pp. 3253–3256.
[46] F. Jin, P. Fieguth, L. Winger, and E. Jernigan, "Adaptive Wiener filtering of noisy images and image sequences," in *Proc. IEEE Int. Conf. Image Process.*, Sep. 2003, vol. 3, pp. 349–352.
[47] M. Kazubek, "Wavelet domain image denoising by thresholding and Wiener filtering," *IEEE Signal Process. Lett.*, vol. 10, no. 11, pp. 324–326, Nov. 2003.
[48] J. S. Lee, I. Jurkevich, P. Dewaele, P. Wambacq, and A. Oosterlinck, "Speckle filtering of synthetic aperture radar images: A review," *Remote Sens. Rev.*, vol. 8, no. 4, pp. 313–340, Jan. 1994.

Sara Parrilli received the Dr. Eng. degree in telecommunications engineering and the Ph.D. degree in electronic and telecommunications engineering from the University of Naples Federico II, Naples, Italy, in 2005 and 2009, respectively.

She is currently an Assistant Researcher with the Department of Biomedical, Electronic, and Telecommunication Engineering, University of Napoli Federico II. Her research activities lie in the area of image processing with particular emphasis on compression and denoising.

Mariana Poderico was born in Naples, Italy, on January 22, 1984. She received the Laurea Specialistica (full marks and laude) degree in telecommunications engineering from the University of Naples Federico II, Naples, in 2008, where she has been working toward the Ph.D. degree in electronic and telecommunication engineering since December 2008.

Her study and research activity focuses on the denoising of SAR images.

Cesario Vincenzo Angelino received the Laurea (M.S.) degree in telecommunication engineering from the University of Naples Federico II, Naples, Italy, in 2006. He is currently working toward the Ph.D. degree in information and communication technologies in a joint program between the University of Nice, Sophia Antipolis, France, and the University of Naples Federico II.

His research activity is in the field of statistical image processing, with attention to digital photography and remote-sensing applications.

Luisa Verdoliva received the Laurea degree in telecommunications engineering and the Ph.D. degree in information engineering from the University of Naples Federico II, Naples, Italy, in 1998 and 2002, respectively.

She is currently a Researcher with the Department of Biomedical, Electronic, and Telecommunication Engineering, University of Naples Federico II. Her current research activity is in image processing, particularly in denoising, wavelet-based techniques, and compression of images.